Sensors & Diagnostics

PAPER

View Article Online
View Journal

Cite this: DOI: 10.1039/d6sd00048g

A molecular switch framework for reagentless electrochemical detection of proteins

Erfan Shirzadi,*[a] Yue Xu,[b] Mara Jenkins,[ae] Jianwen Wang,[ae] Sunandan Tandon,[b] Gyorgy Jaics,[c] Zoya Leonenko[bde] and Mahla Poudineh*[a]

Received 24th February 2026,
Accepted 21st April 2026

DOI: 10.1039/d6sd00048g

rsc.li/sensors

Reagentless electrochemical protein detection is critical for real-time health monitoring. Most currently available electrochemical antibody-based sensors require the addition of external reagents as redox reporters and/or detection antibodies. Here, we introduce ProSwitch, a protein detection sensor that offers an electrochemical and reagentless method of target analyte detection. ProSwitch operates using a molecular switch mechanism, leveraging antibodies and ferrocene-tagged antigens attached to an electrode surface *via* polyethylene glycol (PEG) arms. Protein detection is achieved through an antigen competition strategy, where the target antigen competes with the tagged antigen for binding, generating a measurable electrochemical signal. Tests with various large and small proteins confirmed ProSwitch's broad operational range across diverse proteins, demonstrating its potential suitability for use in biological fluids and health monitoring applications.

Introduction

The capability to measure protein biomarkers in real-time holds transformative potential for healthcare and is critically needed for diagnosis and monitoring of a wide range of diseases, including diabetes, brain trauma injuries, and infections.[1–4] Antibodies are the main recognition elements for protein biomarker detection, which can recognize their specific antigens with high affinity.[5,6] Enzyme-linked immunosorbent assay (ELISA) is the gold standard assay for protein detection; however, it requires a long incubation time and the addition of extra reagents, hindering real-time and reagentless protein detection.[7]

Electrochemical aptamer-based biosensors have recently emerged as a promising tool for reagentless molecular sensing. These sensors operate by leveraging a conformational change in the aptamer, which positions the redox probe near the electrode surface.[8–12] However, selecting aptamers with the desired sensitivity and specificity is a complex and time-intensive process.[11] In contrast, antibodies are more suitable for detecting target proteins, as they have been extensively developed and validated across a broad range of protein biomarkers.

Several other methods have been developed for electrochemical-based protein detection. Electrochemical DNA scaffold sensors operate by detecting a decrease in redox reporter accessibility to the electrode surface upon target binding, which reduces the electrochemical signal.[6,7] Electrochemical proximity assays offer rapid protein detection using a DNA scaffold; target binding introduces steric hindrance, limiting reporter access and thereby decreasing the current. Nucleic acid-modified nanostructure sensors detect proteins through structural changes induced by antigen binding, which alter electron transfer efficiency and generate a measurable electrochemical response.[13,14]

Most electrochemical antibody-based biosensors for protein detection require the addition of extra reagents, such as ferri/ferrocyanide or Prussian blue, for their function.[15,16] Recently, a reagentless, antibody-based electrochemical biosensor has been developed that leverages a molecular pendulum mechanism.[17] This system uses a field effect motion-based molecular pendulum that detects the presence of an antigen through changes in the motion of an antibody/aptamer–DNA assembly. In a more recent study, the molecular pendulum platform was adapted for continuous measurement using voltage oscillations to facilitate the sensor regeneration.[18] While it has been demonstrated for both aptamer and antibody, only the aptamer assay was validated *in vivo*.[18] Another limitation is that most electrochemical methods have been demonstrated for only a narrow range of targets,[18,19] necessitating the development of

[a] *Department of Electrical and Computer Engineering, Faculty of Engineering, University of Waterloo, Waterloo, Ontario N2L 3G1, Canada. E-mail: mahla.poudineh@uwaterloo.ca*
[b] *Department of Physics & Astronomy, University of Waterloo, Waterloo, ON, N2L 3G1, Canada*
[c] *Department of Chemistry, University of Waterloo, Waterloo, Ontario N2L 3G1, Canada*
[d] *Department of Biology, University of Waterloo, Waterloo, ON, N2L 3G1, Canada*
[e] *Waterloo Institute for Nanotechnology, University of Waterloo, Waterloo, ON, N2L 3G1, Canada*

additional detection strategies to establish a truly universal capability.

Alongside electrode-based approaches, nanopore-based electrical protein sensing has also advanced substantially, including magnetic nanoparticle-assisted nanopore blockade for ultrasensitive PSA detection in whole blood, α-hemolysin-nanopore-based ELISA for cancer biomarker analysis, a molecular sandwich/DNAzyme-coupled nanopore strategy for antigen detection, and label-free multianalyte nanopore detection of Alzheimer's disease biomarkers in cerebrospinal fluid and serum.[20–23] These advances highlight the growing interest in electrical protein sensing and suggest that molecular switch concepts could be adapted for point-of-care electrochemical protein detection. A recent work employed a molecular switch assay for fluorescence-based detection of cortisol and digoxigenin.[8] This molecular switch assay has the potential to be adapted for point-of-care electrochemical protein detection.[24]

Here, we postulate developing an antibody-based molecular switch that can toggle between "on" and "off" states in response to the presence of a target antigen. This switching mechanism produces a measurable change in the electrochemical signal, addressing the current need for reagentless electrochemical detection of protein biomarkers. An electrode surface comprising antibody probes and ferrocene (Fc)-tagged antigens (Fc-antigen) linked to the surface *via* polyethylene glycol (PEG) arms was developed. We demonstrated that when the target antigen is present, it competes with the Fc-antigen, causing this tagged antigen to be released. The release can be detected and measured using square wave voltammetry (SWV) (Fig. 1). Thus, the developed biosensor, called ProSwitch, operates without the need to add exogenous reagents. The sensing mechanism uses a molecular switch, driven by the completion of two equilibrium processes: the antibody probe binding to the target antigen and the antibody capturing the Fc-antigen. Additionally, we observed that ProSwitch reaches equilibrium more rapidly, facilitated by the competitive reaction mechanism. In this work, the fabrication of ProSwitch and its thermodynamic modeling and performance are discussed.

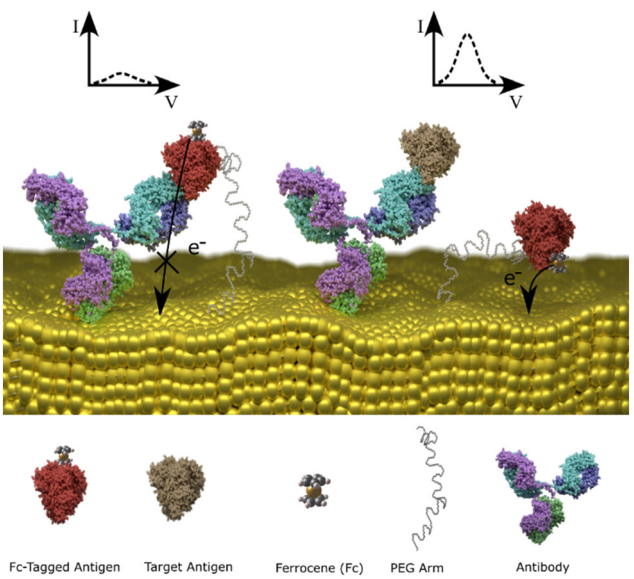

Fig. 1 Overview of ProSwitch biosensor. In the presence of the target antigen, the Fc-antigen is displaced, allowing free Fc-antigens to reach the surface and facilitate charge transfer. Connected to the surface *via* a PEG arm, the Fc-antigen can displace the target antigen and return to its original state, making the system regenerative.

Materials and methods

Materials

Gold Phase Zero electrodes were purchased from Palmsens. *N*-Hydroxysuccinimide (NHS), DI water, thioglycolic acid (TGA), human insulin protein, Amicon Ultra Centrifugal Filters and human serum albumin (HSA) were obtained from Sigma-Aldrich. 1-(3-Dimethylaminopropyl)-3-ethylcarbodiimide hydrochloride (EDC-HCl) and *N*-succinimidyl ferrocenecarboxylate were purchased from TCI chemicals. Monoclonal antibody against insulin (D6C4cc) was purchased from ImmunoDiagnostics Limited. Thrombin monoclonal antibody (5020), human thrombin protein, Slide-A-Lyzer Dialysis Cassettes and phosphate buffer saline (PBS) were purchased from ThermoFischer Scientific. Polyethylene glycol-thiol and NHS conjugates were sourced from Biopharma PEG catalog numbers HE003024-3.4K, HE003024-6K, and HE003024-10K. Anti-human serum albumin antibody [15C7], native human IgG (ab91102) and rabbit anti-human IgG (ab6715) were purchased from abcam.

Synthesis of tagged antigens

400 μl of Native antigen solutions (0.1 mg ml^{-1} 1× PBS) was prepared, then it was reacted with 40 equivalents of PEG-NHS solution prepared in DMSO and 20 equivalents of Fc-NHS in DMSO in the same vial. It was kept in a dark, chilled environment to react for 2.5 hours before purification through filtration and washing. Millipore Centrifugal Filters (0.5 mL with appropriate size cutoff) were prepared by rinsing once to moisten the filter using deionized (DI) water (8000 *cf.*, 7 minutes), then discarding effluent from the tube. Subsequently, 0.5 mL of solute was added and centrifuged (20 000 rcf, 7 minutes), discarding the effluent. Furthermore, it was washed four times with 0.5 mL of 1× PBS with the same centrifuge settings, discarding the effluent after each round, before finally removing the eluate to collect the purified tagged antigen solution. For the purification of 3.4k and 6k insulin, we used Slide-A-Lyzer Dialysis Cassettes with a 3.5k and 10k cutoff, respectively. The concentrated solutions were then analyzed *via* a MALDI-TOF instrument (Bruker Autoflex speed) with an Nd:YAG laser. The matrix used is sinapinic acid in water : acetonitrile with 0.1% TFA.

Biosurface fabrication

The CTI Phase Zero SPE electrode used for biosensor fabrication had screen-printed gold working and counter

electrodes as well as a silver reference electrode. After cleaning the chips with isopropyl alcohol and DI water, a potentiostat was used to apply 5 CV scans from 0–1.3 V *vs.* Ag/AgCl to the electrode to clear organic molecules from the surface. To synthesize active carboxylic acid groups on the gold working electrode surface, a Thioglycolic Acid solution (2 μM) was applied for sixty seconds and then rinsed with DI water. Subsequently, EDC (10 mM)/NHS (20 nM) coupling prepared in a 0.1 M MES (2-(*N*-morpholino)ethanesulfonic acid pH = 5–6) buffer was incubated on the electrode surface for an hour which primed the working electrodes' surface for antibody immobilization.

After washing the electrode surface with 1× PBS, antibodies (0.1 mg mL^{-1}) are quickly deposited on the working electrode surface. While this reaction happens quickly, around 30 minutes in standard conditions, the antibodies were left to incubate in a sealed and chilled environment overnight (~18 hours).

The next day, the electrode was thoroughly rinsed with 1× PBS and the freshly purified tagged antigen solution was added to the working electrode surface. The tagged antigen solution further enabled the creation of a gold biosurface through surface adsorption as a result of Au–S bonds between the thiol groups of the PEG chains and the electrode surface. The electrodes are subsequently sealed and placed in a chilled, darkened environment overnight.

After washing three times with 1× PBS the next day and applying for 5 s the MCH solution in DI water, the electrodes were washed 3 more times with 1× PBS. Next, the chips were treated with different targets at room temperature for 20 minutes. After target incubation, electrochemical experiments were performed.

Electrochemical measurements

Square wave voltammetry and cyclic voltammetry electrochemical experiments were conducted using a Palmsens4 potentiostat, software version PSTrace 5.9.4515.26, and a connection compatible with our three-electrode system. The three-electrode system featured a screen-printed gold working electrode comprising the biosensor, gold as the counter electrode, and mixed silver and silver chloride (Ag/AgCl) as the reference electrode, along with a printed insulating dielectric. Electrochemical measurements recorded using Cyclic Voltammetry (CV) typically had a 0 to +500 mV potential window and V s^{-1} scan rate. Pulsed electrochemical measurements recorded using Square Wave Voltammetry (SWV) had a 100 μA current range and a 0 to +500 mV potential window with a 0.002 step size. Each SWV measurement at increasing native antigen concentrations was taken on a minimum of three working electrodes to produce replicates.

Measurements using rat blood

Rat blood was collected to validate ProSwitch in complex medium. The blood collection was conducted in accordance with the Animal Welfare Act Regulations; all protocols were approved by the University of Waterloo's and McMaster University's Institutional Animal Care and Use Committee. The rat blood samples were obtained from previously collected samples. The animal details (*e.g.*, sex, age, *etc.*) are not available due to the use of previously collected samples.

To obtain the calibration curve for HSA 3.4k in whole rat blood, blood samples spiked with the target analyte were incubated for 15 minutes prior to sensing, and chips were thoroughly washed before each concentration point to minimize the effects of sensor fouling due to blood clogging.

Thiol coverage determination

Surface coverage of HSA-6k was determined using a procedure similar to that described by Calvente *et al.*[25] The geometric surface area was 0.0314 cm^2. The devices were dipped in 10 mM NaOH, and reductive desorption measurements were performed in 10 mM NaOH. This solution was degassed with N_2(g) for 10 min, and cyclic voltammograms were recorded under an N_2 atmosphere.

$$\text{Au-SR} + e^- \rightarrow \text{Au} + RS^-$$

Sample preparation for AFM

We used the same method as the preparation of the biofilm fabrication, excluding the CV cycles for making the AFM samples on a 200 nM evaporated gold on silicon wafers as the substrate.

Atomic force microscopy measurement

Atomic force microscopy was utilized to obtain the surface structure and topological information of the samples. In this study, dry biosensor surfaces were imaged by JPK Nanowizard II (Bruker, Germany). PPP-NCH silicon probes (NanoSensors, Switzerland) with 42 N m^{-1} spring constant scanned the sample surfaces in the air in the intermittent-contact mode at the resonance frequency 290–300 kHz. Images obtained by JPK were processed by Gwyddion software (2.66).

Localized surface plasmon resonance spectroscopy (LSPR)

The binding of HSA antigen and HSA-tagged antigen to HSA antibody was detected by OpenSPR 3.0 instrument (Nicoya Lifesciences, Canada) and recorded by Nicoya Lifesciences software 3.11.

Surface modification of gold sensors

The gold sensors (Nicoya Lifesciences, Canada) were immobilized using a similar method to the preparation of biofilm, excluding the CV cleaning cycles.

LSPR Experiment setup

The LSPR system was infused with PBS buffer (pH 7.4) during the entire experiment. The PBS buffer flowed over the functionalized biosensor surface consistently at a certain flow

rate. The injection of solutions with ingredients different from the PBS buffer would induce the wavelength shift shown in the LSPR software.

At the beginning of the experiments, with a 150 μL min^{-1} flow rate, the 200 μL DI water was injected into the system twice to make sure the excess bubbles were removed. Then, the flow rate was turned to 50 μL min^{-1} for the injection of agents in the following order and steps: 100 μL 1 μl HSA dissolved in PBS buffer was injected, and waited for 25–30 min for the proteins' binding and dissociation from the receptors. 200 μL 200 mM Glycine solution (in 1× PBS) was injected for regeneration, and step 1 was repeated.

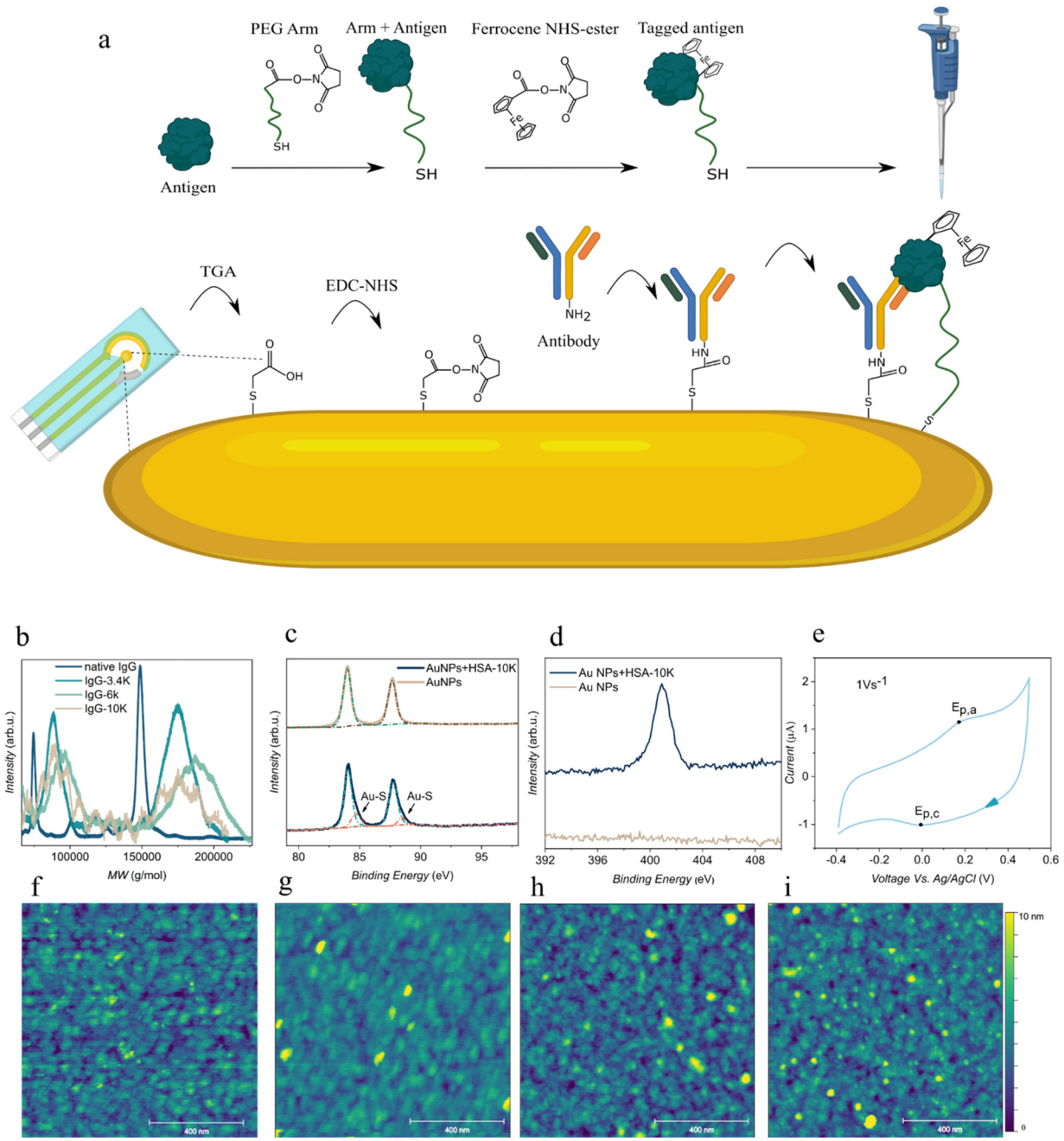

Fig. 2 Biosensor fabrication and characterization. a, Scheme showing the steps for the fabrication of ProSwitch biosensor. b, The MALDI-TOF spectra of IgG antigen with three different arm sizes. Each peak in the spectra represents a specific number of arms attached to the antigen. c, Au4f XPS spectra of bare gold nanoparticles (Au NPs) and gold nanoparticles with HSA-10k (AuNPs + HSA-10k). The dashed lines indicate the fitted results. d, N1s XPS spectra show the presence of protein for AuNPs + HSA-10k (after washing), suggesting the covalent attachment of the antigen to the gold surface. e, CV scanning identifying the presence of ferrocene redox tag for Fc-HSA-10k. The scan rate was 1 V s^{-1} and 1× PBS buffer was used. Ep,a and Ep,c refer to anodic and cathodic potentials, respectively. Lower panel: The AFM topography images of f, bare gold surface, gold with g, HSA-10k, h, anti-HSA antibody, and i, HSA-10k + anti-HSA antibody.

Results and discussion

Fabrication and characterization of ProSwitch

To fabricate the ProSwitch (Fig. 2a), the gold working electrode of commercially available screen-printed three-electrode chips was modified with thioglycolic acid (TGA) to introduce the carboxylic acid groups. Next, the carboxylic acid group was activated *via* 1-ethyl-3-(-3-dimethylaminopropyl) carbodiimide hydrochloride/*N*-hydroxysuccinimide (EDC/NHS) chemistry for functionalizing the surface with antibodies against the desired target antigens. Two distinct strategies were employed for surface immobilization. A PEG linker modified with a thiol anchor was used to attach the labeled antigen to the surface, while the antibody was immobilized using a combination of thiol and EDC/NHS chemistry. In the presence of free antigen, the labeled antigen is competitively displaced, and the PEG linker facilitates the free movement of the Fc-labeled antigen upon release, thereby generating an electrochemical signal. Adding PEG linkers further improves sensor performance by providing anti-fouling properties and resistance to DNase-mediated degradation compared to DNA-linker immobilization strategies.[26,27] This makes the platform suitable for use in biological fluids.

Fc-tagged antigens linked to PEG arms were prepared by reacting the NHS-ester of the Fc redox reporter with thiolated PEG arms and native antigens in a 1× PBS buffer, followed by a purification step. Subsequently, Fc-antigen was added to the working electrode, where the antibody was already immobilized. Three PEG linkers with molecular weights of approximately 3400 Da, 6000 Da, and 10 000 Da were used, referred to as 3.4k, 6k, and 10k arms, respectively. Fig. 2b shows the matrix-assisted laser desorption/ionization time-of-flight (MALDI-TOF) spectra of the modified Fc-IgG antigen with three different PEG sizes. The mass spectra indicate multiple attachments of arms depending on the reaction concentrations and the reactivity of each PEG linker. The degree of modification ranges from 1–3 for the 10k arms to 2–6 for 6k and 1–8 for 3.4k arms (Fig. S1).

To examine the binding of Fc-antigens linked with the PEG-thiolated arms to the gold surface, gold nanoparticles coated with the human serum albumin (HSA) antigens modified with 10k PEG arm (HSA-10k) were characterized *via* X-ray photoelectron spectroscopy (XPS; Fig. 2c). It is known that thiol groups are likely to bind to gold and copper surfaces.[28,29] Comparing Au4f XPS spectra of bare gold nanoparticles and gold nanoparticles coated with HSA-10k indicates a shoulder at 84.7 and 88.5 eV attributed to the formation of Au–S bonds.[28,30,31] Moreover, comparing the N1s XPS of protein-capped gold nanoparticles with uncoated gold nanoparticles indicates the presence of organic compounds (protein/antigen) (Fig. 2d). The XPS results indicate the reaction of the thiol-containing tagged antigen with the gold surface. A similar outcome is expected when the tagged antigen linked with the PEG arm is added to the gold working electrode of the chips.

To verify the reaction of NHS-ester of ferrocene with antigen, cyclic voltammetry (CV) scanning was performed using an electrode modified with Fc-HSA linked to the 10k PEG arm (Fc-HSA-10k). Peaks assigned to the ferrocene redox at approximately 0.2–0.4 V *vs.* Ag/AgCl reference electrode were observed (Fig. 2e).[32,33]

Next, atomic force microscopy (AFM) scanning was used to investigate the surface coverage. Silicon wafers coated with 300 nm of gold were used as the substrate for AFM imaging instead of the commercial chip, as the actual working electrode surface was too rough for reliable AFM imaging (Fig. S2). Analysis of AFM images of the bare gold surface reveals a relatively rough texture with peaks as high as 2–3 nm (Fig. 2f). In the AFM image of Fc-HSA-10k deposited on the gold surface, peaks as high as 6–8 nm are observed, which aligns with the expected measures reported for HSA (Fig. 2g).[34] The antibody-coated gold surface exhibits peaks as high as 8–9 nm, suggesting a relatively upright orientation of antibodies at these spots (Fig. 2h). The gold surface coated with both Fc-HSA-10k and antibody showed greater protein coverage (Fig. 2i). Moreover, the spot diameters were smaller, indicating the formation of more individual HSA-10k + anti-HSA antibody assemblies. The peak height ranges from 5–7 nm, which is comparable to the size of HSA and lower than that of the antibody-only surface, suggesting that the interaction of HSA-10k with the antibody causes a slight tilt in the anti-HSA antibody. Although AFM results show a dry-state height of 6–8 nm for Fc-HSA-10k, the PEG linkers have at least a Flory radius of at least 4.7 nm in solution and remain highly flexible, allowing the tethered HSA to extend beyond the measured dried-layer height and access the antibody binding sites. We also observed the presence of protein aggregates, particularly on the antibody-only or HSA-10k-only surfaces, likely due to the accumulation of antibodies or HSA antigens.

Coupling *via* EDC–NHS typically results in a random orientation of antibodies on the surface.[35] However, performing the coupling reaction at a more neutral pH (as in our Method) has been shown to increase exposure of the Fab region, suggesting a more upright orientation.[36] In addition, the AFM results in Fig. 2h (antibody-covered gold) compared to Fig. 2f (clean gold) show a height of approximately 8–9 nm in the presence of antibody, which is consistent with the expected height of antibodies and supports an upright antibody orientation.

ProSwitch sensing strategy

Next, we studied the reagentless sensing mechanism of the ProSwitch assay by combining thermodynamic analysis and surface plasmon resonance (SPR) to determine the target analyte's median effective concentration (EC_{50}). In this system, the Fc-antigen is tethered to the electrode surface *via* a PEG arm linker, allowing the Fc-antigen to remain accessible for interaction with the antibody. The target antigen then competes with the Fc-antigen for binding to the immobilized antibody (Fig. 3a). Thus, the Fc-antigen alternates between an "off" state, where it binds to the

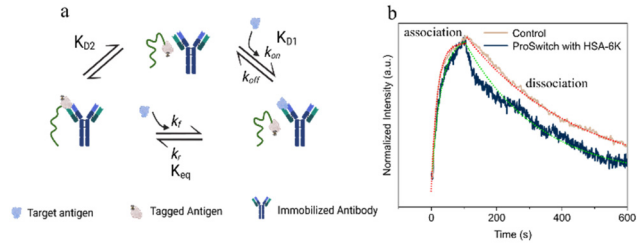

Fig. 3 Antigen–antibody equilibrium. a, Scheme showing the equilibrium between the target antigen and the tagged antigen. b, SPR results show a slower association and a faster dissociation of HSA in the ProSwitch electrode. The fitted data is shown with dotted lines.

antibody, and an "on" state, where it is free to diffuse toward the surface, generating an electrochemical signal.

The ProSwitch assay is inherently reagentless because the redox reporter, ferrocene, is integrated directly into the biosensor, enabling target detection without the need for additional reagents. Under equilibrium conditions, the following reactions occur:

$$\mathrm{AGNAB} \Leftrightarrow \mathrm{AGN} + \mathrm{AB} \quad K_{\mathrm{D1}} = \frac{[\mathrm{AGN}][\mathrm{AB}]}{[\mathrm{AGNAB}]} \tag{1}$$

$$\mathrm{AGN^*AB} \Leftrightarrow \mathrm{AGN^*} + \mathrm{AB} \quad K_{\mathrm{D2}} = \frac{[\mathrm{AGN^*}][\mathrm{AB}]}{[\mathrm{AGN^*AB}]} \tag{2}$$

Where [AGN] and [AGN*] indicate the target antigen and Fc-antigen concentrations, respectively. [AGNAB] and [AGN*AB] show the concentrations (coverage) of target antigen–antibody and Fc-antigen–antibody complexes, respectively. The resultant equilibrium condition, thus, can be determined as follows:

$$\mathrm{AGN\ (aq)} + \mathrm{AGN^*AB\ (ads)} \Leftrightarrow \mathrm{AGNAB\ (ads)} + \mathrm{AGN^*\ (ads)}$$

$$K_{\mathrm{eq}} = K_{\mathrm{D2}}/K_{\mathrm{D1}} = \frac{k_{\mathrm{f}}}{k_{\mathrm{r}}} = \frac{[\mathrm{AGNAB}][\mathrm{AGN^*}]}{[\mathrm{AGN}][\mathrm{AGN^*AB}]} \tag{3}$$

At the EC_{50} point, it is assumed that the concentration of [AGN*AB] equals that of [AGNAB]. Therefore, the EC_{50} can be calculated using the equation below:

$$EC_{50} = [\mathrm{AGN}]_{0.5} = 1/K^*_{\mathrm{eq}}[\mathrm{AGN^*}]_{0.5} \tag{4}$$

Where $[AGN]_{0.5}$ and $[AGN^*]_{0.5}$ show the concentrations of the target antigen and the Fc-antigen at the median effective point. To calculate the EC_{50}, the value of $[AGN^*]_{0.5}$ was estimated using the approach outlined below, while K_{eq} was measured through SPR, as described in the subsequent section.

Estimation of Fc-antigen concentration at median effective point ($[AGN^*]_{0.5}$)

Fc-antigen is bound to the surface; thus, its concentration can be driven from the below equation outlined previously:[32]

$$[\mathrm{AGN^*}]_{0.5} = \Gamma\mathrm{AGN}^*_{0.5}/L \tag{5}$$

Where $\Gamma AGN^*_{0.5}$ is the surface coverage of the Fc-antigen at EC_{50} and L is the sum of AGN size with the Flory radius of the arm.[32] The Flory radius estimations were presented in Table S1.

The charge transferred (Q) during CV measurement, conducted at a scan rate of 1 V s^{-1}, was used to determine $\Gamma GN^*_{0.5}$ using the following equation:

$$\Gamma\mathrm{AGN}^*_{0.5} = Q/nFA \tag{6}$$

Where F is the Faraday number, A is the surface area, and n = 2 is the number of ferrocenes in the tagged antigen (see Fig. S3 for determination of n). As an example, the surface coverage of Fc-antigen was calculated for the HSA-6k sample as $\Gamma AGN^*_{0.5} = 3.2 \pm 1.5 \times 10^{-12}$ mol cm^{-2} and therefore using eqn (5), $[AGN^*]_{0.5} = 2.8 \pm 1.2 \times 10^{-3}$ M, (see Table S1). The total thiol coverage for HSA-6k, indicating the coverage of all thiol species (Antibody, AGN*, TGA), is determined as $4.6 \pm 2 \times 10^{-11}$ mol cm^{-2} using the reductive stripping method described earlier (Fig. S4).[25] Which is about 10 times larger than the coverage of the tagged antigen at EC_{50} ($\Gamma AGN^*_{0.5} = 3.2 \pm 1.5 \times 10^{-12}$ mol cm^{-2}).

Estimation of the equilibrium dissociation constant (K_{eq})

To estimate K_{eq}, SPR analysis was conducted using a complete assay, which included the Fc-antigen linked to the surface and the immobilized antibody. Additionally, a control assay without the Fc-antigen was performed. As an example, the HSA-6k sensing mechanism was studied to estimate the K_{eq} (Fig. 3b). We assumed that the SPR measurements for the HSA-6k sample primarily show the association and dissociation rates of eqn (3). Therefore, to determine these rates, the HSA-6k SPR data were analyzed by fitting them to the following equations:

$$\frac{R_t}{R_{\mathrm{eq}}} = 1 - e^{-(k_{\mathrm{f}}[\mathrm{AGN}] + k_{\mathrm{r}}[\mathrm{AGN^*}])t} \tag{7}$$

$$\frac{R_t}{R_{\mathrm{eq}}} = e^{-k_{\mathrm{r}}[\mathrm{AGN^*}]t} \tag{8}$$

Where k_f and k_r are forward and reverse rates of the full assay described by eqn (3), respectively, $k_r[AGN^*]$ is fitted reverse rate, $k_f[AGN] + k_r[AGN^*]$ is fitted forward rate, R_t is the SPR response at time t, and R_{eq} is the response at equilibrium, which in this case:

$$R_{\mathrm{eq}} = \frac{R_{\mathrm{max}}[\mathrm{AGN}]}{[\mathrm{AGN}] + K_{\mathrm{eq}}[\mathrm{AGN^*}]}. \tag{9}$$

R_{max} is the maximum SPR response when the target antigen replaces all the tagged antigens.

We used [HSA] = 1 μM in the SPR experiments and based on the fitting results, the forward association rate was determined as $k_f = 3.4 \pm 0.1 \times 10^4$ M^{-1} s^{-1}. For simplicity, the $[AGN^*]_{0.5}$ = ($2.8 \pm 1.2 \times 10^{-3}$ M) concentration was used for variable [AGN*]. Thus, the reverse rate was measured as the following:

$$k_r = \text{fitted reverse rate}/[\text{AGN}^*]_{0.5} = (3.7 \pm 0.1 \times 10^{-3}\ \text{s}^{-1})/(2.8 \pm 1.2 \times 10^{-3}\ \text{M}) = 1.4 \pm 0.3\ \text{M}^{-1}\ \text{s}^{-1}.$$

Thus, K_{eq} was calculated as:

$$K_{eq} = \frac{k_f}{k_r} = \frac{k_{D2}}{k_{D1}} = 2.4 \pm 0.5 \times 10^4 \quad (10)$$

SPR experiments were conducted to compare ferrocene-only tagged HSA (without the PEG arm) with native HSA as a control (Fig. S5). The native HSA exhibited a dissociation constant (K_{D1}) of 4.6×10^{-8} M, whereas the ferrocene-only tagged HSA showed a weaker binding affinity, with a K_D of 21×10^{-8} M. These results indicate that the tagging reduces the antigen's affinity for the antibody, likely due to steric or conformational effects. This lower affinity allows the tagged antigen to be competitively displaced by the higher-affinity free antigen. Importantly, although the tagged protein can still bind to the antibody, its reduced binding strength makes it susceptible to replacement by the free analyte, enabling the competitive switching mechanism central to our assay design.

We also compared the binding and dissociation of HSA to HSA antibody-coated gold nanoparticles with and without (control) Fc-antigen. For the control sample, an association rate of $5.2 \pm 0.2 \times 10^4$ M^{-1} s^{-1} and a dissociation rate of $2.4 \pm 0.1 \times 10^{-3}$ s^{-1} was calculated (Fig. 3b and Table 1). These results show that the HSA-6k full assay has a slower association rate (k_f) and a faster dissociation rate (k_r) compared to the control sample (Fig. 3b and Table 1). One should highlight that this system only works as a real-time sensor when there is a fast dissociation of the antibody–antigen, a limitation that is inherited from the low K_D values of antibodies.[18,37]

Considering $[\text{AGN}^*]_{0.5} = 2.8 \pm 1.2 \times 10^{-3}$ M and using eqn (4), EC_{50} was calculated as 1.2×10^{-7} M. It is important to note that the calculated EC_{50} was higher than the experimental results (see next section), which could be attributed to an underestimation of K_{eq} obtained from SPR measurements. Specifically, from calculated association and dissociation rates, K_{D1} was determined as $K_{D1} = 4.6 \pm 0.3 \times 10^{-8}$ M, which is significantly larger than the expected K_D for a monoclonal antibody. While SPR was used to characterize the interaction between the antibody and ferrocene-labeled *versus* native antigen, it is important to note that these measurements were intended for relative comparison only. The dissociation constant obtained from SPR ($4.6 \pm 0.3 \times 10^{-8}$ M) was significantly higher than the affinity that is expected from a monoclonal antibody used in ELISA. This discrepancy aligns with previous findings that SPR often underestimates binding affinity due to mass transport limitations and surface immobilization artifacts, particularly in systems involving high-affinity monoclonal antibodies.[38] Therefore, we did not rely on the SPR-derived constants for equilibrium modeling or EC_{50} calculations in this study. Instead, the SPR data serve as qualitative evidence to illustrate altered binding dynamics following antigen modification, not as definitive quantitative binding metrics.

In vitro validation of ProSwitch assay

We next examined ProSwitch assay for the detection of different target proteins. A ProSwitch assay for HSA detection using Fc-HSA-3.4k and anti-HSA antibody was prepared. We used square wave voltammetry (SWV) as a sensitive method to measure the charge transfer. As shown in Fig. 4a, an increase in SWV peak current was observed with increasing HSA concentration. When an antigen without a PEG arm was used, a decay in the signal was observed, indicating the detachment of the antigen without PEG arms (Fig. S6). Therefore, the PEG linker is crucial for creating a regenerative biosensor.

To investigate the cause of the current increase in the presence of the target antigen, the ratio of the SWV peak current to frequency (I/f) was plotted against frequency (Fig. 4b). The results can be fitted with a parabola function where the frequency at which the maximum of I/f is located is linearly related to the electron transfer rate.[39–41] Therefore, the electron transfer rate is relatively constant across different concentrations of HSA (Table S2). The surface electron transfer rate is also inversely related to the distance of the tagged antigen to the gold surface.[32] Thus, the average distance of Fc-antigens from the gold surface is constant. Therefore, the increase in SWV current can be attributed to the displacement of a greater number of tagged antigens by the target antigens. In our system, consistent with the results in Fig. 4b, we hypothesize that there is negligible electron transfer in the bound state when the antibody–tagged antigen complex is oriented upright on the surface. Accordingly, the current observed in the presence of the target antigen primarily arises from displaced, freely tagged antigen. As the target antigen concentration increases, it competitively displaces more tagged antigen, increasing the amount of free tagged antigen and thus the SWV peak current. This interpretation is consistent with Fig. 1, which indicates that no electron transfer occurs between the surface and the tagged antigen while it remains bound to an antibody. However, if the antibody adopts a flatter orientation on the surface, the attached tagged antigen may still access the electrode and undergo electron transfer, potentially in a manner similar to a free tagged antigen. We attribute the

Table 1 Summary of data obtained from SPR. The standard deviations are calculated for at least three replicates ($n \geq 3$)

	Fitted forward rate (M^{-1} s^{-1})	Fitted reverse rate (s^{-1})
Control (native HSA)	$5.2 \pm 0.2 \times 10^4$	$2.4 \pm 1.4 \times 10^{-3}$
HSA-6k	$3.4 \pm 0.1 \times 10^4$	$3.7 \pm 0.1 \times 10^{-3}$

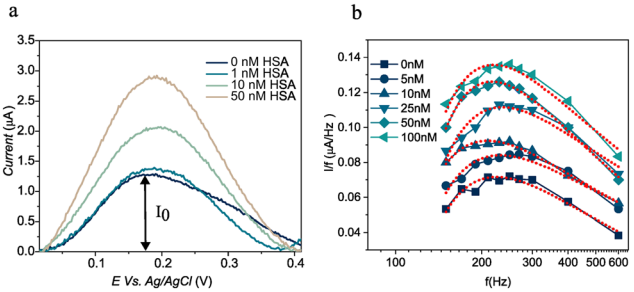

Fig. 4 a, Square wave voltammetry measurements showing an increase in the peak height in the presence of HSA measured at 150 Hz. b, The current to frequency ratio shows a parabola dependency peaking at approximately 200 Hz for Fc-HSA-6k. The dotted line shows the fitting results.

negligible baseline signal at 0 nM to this surface-induced "lying-flat" population.

Next, the ProSwitch assay was examined for detecting insulin (INS), human thrombin protein (Thr), HSA, and IgG using their specific antibodies and their specific Fc-antigen linked with different PEG arm sizes (Fig. 5a–l). While the Au–S bond is relatively strong, the surface coverage of both the antibody and the tagged antigen may differ between devices. To account for this variability, we normalized the current response to I_0.

To fit the experimental data with a dose–response curve, the following equation was achieved based on the model described earlier (see SI Text):

$$\theta = \frac{[\mathrm{AGN}]\left(\sqrt{\left(1+\frac{8\times \mathrm{EC}_{50}}{[\mathrm{AGN}]}\right)}-1\right)}{4\times \mathrm{EC}_{50}} \quad (11)$$

Where θ is the fraction of occupied antibodies with the target antigen to the total occupied antibodies with target and Fc-antigens. This equation resembles a sigmoidal curve and compares with Monod and Hill's equation ($n \geq 1$),[42] it has a less steep "linear range" (Fig. S7). For all tested targets, a broader dynamic range was observed compared to the typical dose–response curves of antibody-based assays. Similar behavior was also observed for the detection of small protein molecules using antibodies in the previously reported fluorescence-based molecular switch assay.[8] The full comparison of eqn (11) to the Hill and Monod equations is presented in Table S3.

Sigmoidal dose–response curves were achieved for different protein targets. We observed that the median effective concentrations (EC_{50}) of ProSwitch assays with the 3.4k arm

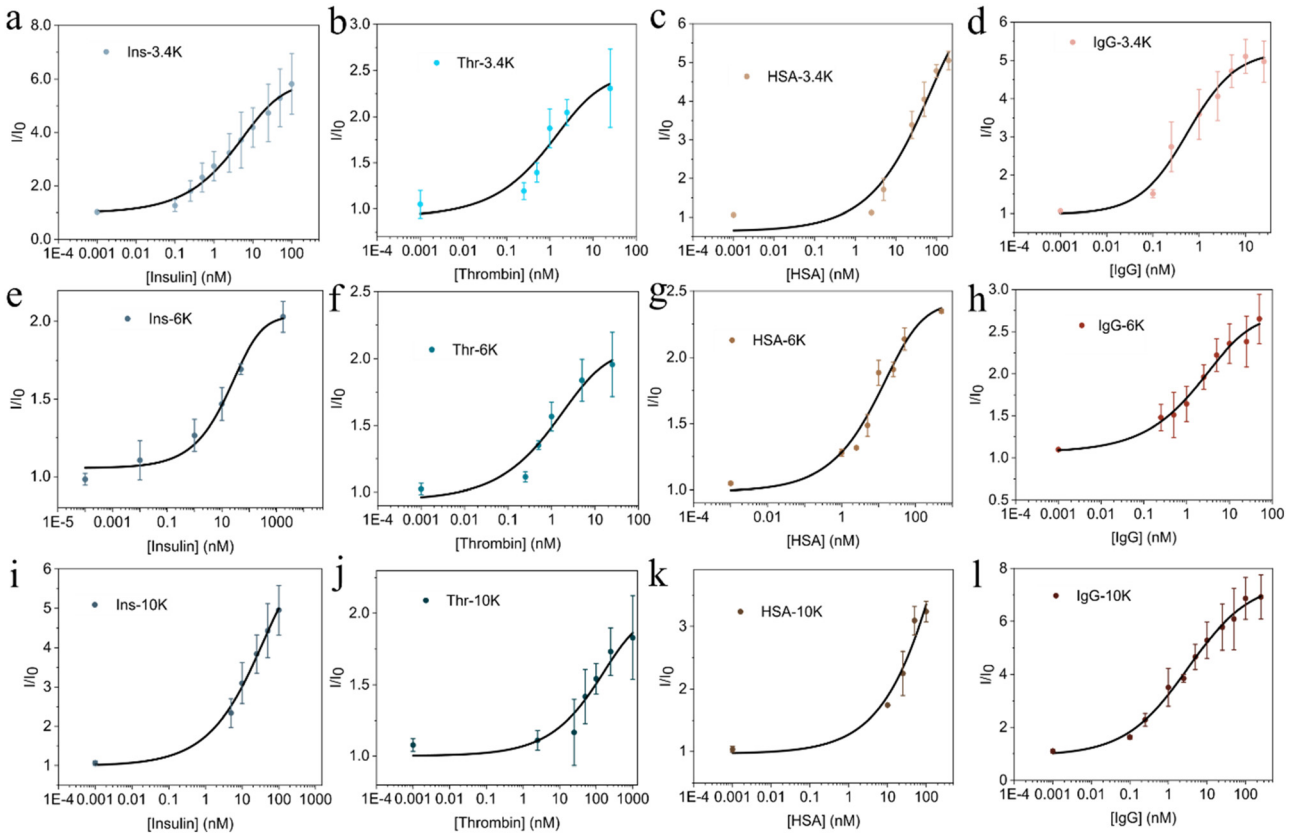

Fig. 5 Dose–response curves. The dose–response curve for proteins with a–d, 3.4k arm, e–h, 6k arm, and i–l, 10k arm. All the measurements were performed in 1× PBS buffer, and a 20 minute incubation time was used for each concentration point. The curves represent the fittings based on eqn (11). The error bars show standard deviation for at least three replicates ($n \geq 3$).

generally occur at lower target concentrations compared to those with the 10k arm. This difference may be attributed to fewer degrees of modification when the 10k PEG is used compared to the 3.4k and 6k PEG arms (Fig. 2b). As a result, a larger K_{D2} is expected, which, according to eqn (4), shifts the EC_{50} to a higher concentration. For several dose–response curves (specifically in panels 5c and i–k), data points in the sub-nanomolar range (0.001 nM to 1 nM) were not included, as preliminary experiments indicated that these concentrations did not elicit a significant or reproducible analytical response above the baseline noise.

The specificity of the ProSwitch assay toward the target protein was tested for all the target proteins. The results shown in Fig. 6 indicate the high specificity of the assay, originating from the strong preference of the monoclonal antibodies for their target antigen. This highlights the potential applicability of ProSwitch in complex biological fluids, such as blood and interstitial fluid.

We conducted additional experiments to monitor the response of the HSA-3.4k ProSwitch sensor at higher temporal resolution. Specifically, we measured the sensor signal every 5 minutes during the first 30 minutes, and every 15 minutes thereafter, for a total duration of 75 minutes, using 100 nM HSA spiked into 1× PBS. Fig. 6b indicates that the sensor remains sufficiently stable throughout the experiment. Additionally, the stability of the HSA-3.4k ProSwitch assay was assessed by measuring the sensor response at a 0 nM concentration over more than 25 measurements taken at 20 minute intervals (Fig. S8). The results demonstrated high stability, with less than 20% variation in response. The stability of the ProSwitch was evaluated over a 7 day period. ProSwitch devices were fabricated using HSA-3.4k and stored at 4 °C for 1, 3, 5, or 7 days. On each day, the sensor response was measured in 1× PBS buffer. The results demonstrate that the sensor remains stable without use for at least 7 days (Fig. 6c).

Measurement in spiked whole blood samples

As the next step, we evaluated the performance of ProSwitch for measuring target concentration in whole blood samples using HSA ProSwitch devices. Whole blood samples were spiked with different concentrations of HSA, and electrochemical measurements were performed to generate a titration curve (Fig. 6d). Since the antibody used in this study is specific to human serum albumin, we do not expect any significant contribution from rat serum albumin. We also calculated the limit of detection (LOD) for the ProSwitch sensor in both buffer and whole blood, which were 16 nM and 132 nM, respectively. As expected, the LOD is higher (*i.e.*, sensitivity is lower) in whole blood compared to buffer, consistent with the increased complexity and potential for fouling in blood.[26]

Discussion

By combining a molecular switch with antibody-based target recognition, ProSwitch offers a flexible and broadly applicable sensing framework. The competition-driven antigen displacement

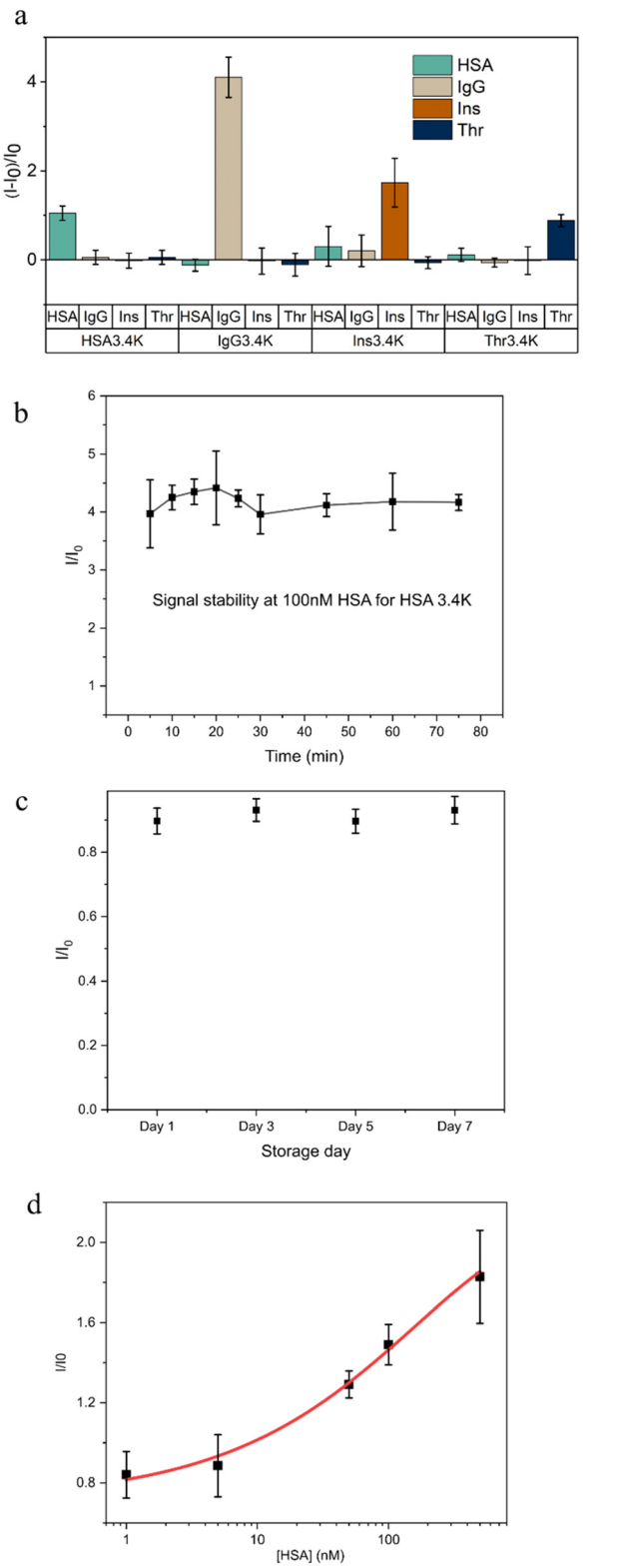

Fig. 6 Specificity and stability measurements. a, Specificity test of ProSwitch assay against three proteins with 10 nM concentration in 1× PBS buffer (n = 3). b, Signal stability for 100 nM HSA for HSA 3.4k devices (n = 3) for PBS buffer. c, The storage stability of HSA-3.4k. The measurements are performed in 1× PBS buffer (0 nM HSA) on separate chips. d, The titration curve for HSA-3.4k in whole rat blood.

mechanism further enables reagent-free protein quantification, eliminating the need for exogenous reagents during measurement. Our future work will assess sensor performance in clinically relevant complex samples—whole blood, plasma, and interstitial fluid—to enable point-of-care and wearable applications. To support repeated measurement and for targets requiring higher-affinity antibodies, we will pursue integration of the competitive molecular switch with regenerable sensing modalities (*e.g.*, active reset systems).[18,37]

Our method imposes several limitations: one key limitation is that the target protein must contain at least two amine groups that can participate in EDC-NHS chemistry: one for attaching ferrocene and the other for the PEG arm. If the protein does not have these available amine groups, alternative functionalization methods will be needed. Larger target proteins typically have more surface lysines, which increases the likelihood of having additional amine groups for modification. On the other hand, a more robust approach is to attach the PEG linker to specific sites on the antibody rather than the gold surface, to ensure greater control over the coverage of the tagged antigen and its distance from the antibody, as at the current configuration, we lack control over coverage and distance of the antibody to the tagged antigen. This way ensures the 1 : 1 ratio of tagged antigen : antibody and a controlled distance between the tagged antigen and the antibody.

Conclusions

The use of the molecular switch and antibody-based recognition provides the ProSwitch sensor with flexibility and broad applicability. Additionally, the competition-based antigen displacement strategy enables measurement of protein concentrations without requiring the addition of external reagents. The incorporation of PEG linkers further enhances the sensor's performance by offering anti-fouling properties and resistance to DNase degradation (compared with a DNA linker strategy for the immobilization), making the system suited for use in biological fluids.[26]

Author contributions

The manuscript was written through the contributions of all authors. All authors have given approval to the final version of the manuscript.

Conflicts of interest

There are no conflicts to declare.

Data availability

The data supporting this article have been included as part of the manuscript and supplementary information (SI). Further information can be inquired directly from the corresponding author.

Supplementary information: SI file contain model derivations, protein and electrode characterization, electrochemical measurements, and stability data. It includes MALDI, AFM, SPR, CV, and SWV results, along with tables on PEG arm size, electron-transfer rates, and comparison of the proposed response model with Monod and Hill equations. See DOI: https://doi.org/10.1039/d6sd00048g.

Acknowledgements

We thank Dr. Valerie Goodfellow for assisting with mass spectrometry measurements and analysis, Dr. Joseph Thomas for performing XPS measurements, and Prof. Pavle Radovanovic for using his laboratory equipment. We also acknowledge the Schertzer lab and Dr. Nicole Barra for providing rat blood. We thank the University of Waterloo's AMTD Waterloo Global Talent Postdoctoral Fellowship and Interdisciplinary Trailblazer Award. We acknowledge funding from Natural Science and Engineering Research Council (NSERC) of Canada and Canadian Foundation for Innovation (CFI).

References

1 F. B. Yihunie, M. A. Belete, G. Fentahun, S. Getachew and T. Dubie, *Adv. Cell Gene Ther.*, 2023, **2023**, 5510791.
2 D. B. Hier, T. Obafemi-Ajayi, M. S. Thimgan, G. R. Olbricht, S. Azizi, B. Allen, B. A. Hadi and D. C. Wunsch, *Biomark. Res.*, 2021, **9**, 1–17.
3 K.-A. Spencer, F. A. Osorio and J. A. Hiscox, *Vaccine*, 2007, **25**, 5653–5659.
4 N. R. Sproston and J. J. Ashworth, *Front. Immunol.*, 2018, **9**, 754.
5 R. L. Reaño and E. C. Escobar, *Front. Bioeng. Biotechnol.*, 2024, **12**, 1361469.
6 R. M. Madiona, N. G. Welch, J. A. Scoble, B. W. Muir and P. J. Pigram, *Biointerphases*, 2017, **12**, 031007.
7 S. Hosseini, P. Vázquez-Villegas, M. Rito-Palomares, S. O. Martinez-Chapa, S. Hosseini, P. Vázquez-Villegas, M. Rito-Palomares and S. O. Martinez-Chapa, in *Enzyme-Linked Immunosorbent Assay from A to Z*, Springer, 2018, ch. Advantages, Disadvantages and Modifications of Conventional ELISA, pp. 67–115.
8 I. A. Thompson, J. Saunders, L. Zheng, A. A. Hariri, N. Maganzini, A. P. Cartwright, J. Pan, S. Yee, C. Dory and M. Eisenstein, *Sci. Adv.*, 2023, **9**, eadh4978.
9 S. Song, L. Wang, J. Li, C. Fan and J. Zhao, *TrAC, Trends Anal. Chem.*, 2008, **27**, 108–117.
10 B. Strehlitz, N. Nikolaus and R. Stoltenburg, *Sensors*, 2008, **8**, 4296–4307.
11 M. McKeague and M. C. DeRosa, *J. Nucleic Acids*, 2012, **2012**, 748913.
12 É. V. d'Astous and P. Dauphin-Ducharme, *Chem. Commun.*, 2024, **60**, 6419–6422.
13 S. Somasundaram and C. J. Easley, *J. Am. Chem. Soc.*, 2019, **141**, 11721–11726.

14 A. Gurukandure, S. Somasundaram, A. S. Kurian, N. Khuda and C. J. Easley, *Anal. Chem.*, 2023, **95**, 18122–18129.
15 G. Ozcelikay, F. Mollarasouli, M. A. Unal, K. Gucuyener and S. A. Ozkan, *Biosensors*, 2022, **12**, 1165.
16 D. Yang, J. Ran, H. Yi, P. Feng and B. Liu, *Sensors*, 2023, **23**, 9029.
17 J. Das, S. Gomis, J. B. Chen, H. Yousefi, S. Ahmed, A. Mahmud, W. Zhou, E. H. Sargent and S. O. Kelley, *Nat. Chem.*, 2021, **13**, 428–434.
18 H. Zargartalebi, S. Mirzaie, A. GhavamiNejad, S. Ahmed, F. Esmaeili, A. Geraili, C. Flynn, D. Chang, J. Das and A. Abdrabou, *Science*, 2024, **386**, 1146–1153.
19 Z. Wu, S. E. Isaacson, C. D. Flynn, J. Das and S. O. Kelley, *Acc. Chem. Res.*, 2025, 428–434.
20 K. Chuah, Y. Wu, S. Vivekchand, K. Gaus, P. J. Reece, A. P. Micolich and J. J. Gooding, *Nat. Commun.*, 2019, **10**, 2109.
21 Q. Liu, Y. Ouyang, Y. Wang, S. Zhou, Y. Zhan and L. Wang, *Adv. Healthcare Mater.*, 2025, **14**, 2405058.
22 L. Wang, S. Zhou, Y. Wang, Y. Wang, J. Li, X. Chen, D. Zhou, L. Liang, B. Yin and Y. Zhang, *Faraday Discuss.*, 2025, **257**, 60–72.
23 Y. Yi, P. Song, Z. Li, J. Ju, G. Sun, Q. Ren, K. Zhou, L. Liu and H.-C. Wu, *Nat. Nanotechnol.*, 2025, **20**, 1079–1086.
24 E. Shirzadi, M. Huynh, P. GhavamiNejad, H. Zheng, A. Saini, F. Bakhshandeh, F. Keyvani, D. Mantaila, F. A. Rahman and J. Quadrilatero, *Adv. Sens. Res.*, 2023, 2300122.
25 J. J. Calvente, Z. Kováčová, M. D. Sanchez, R. Andreu and W. R. Fawcett, *Langmuir*, 1996, **12**, 5696–5703.
26 S. Saxena, P. Sen, L. Soleymani and T. Hoare, *Adv. Sens. Res.*, 2024, **3**, 2300170.
27 E. b. Jarosińska, Z. Zambrowska and E. Witkowska Nery, *ACS Omega*, 2024, **9**, 4572–4580.
28 E. Shirzadi, Q. Jin, A. S. Zeraati, R. Dorakhan, T. J. Goncalves, J. Abed, B.-H. Lee, A. S. Rasouli, J. Wicks and J. Zhang, *Nat. Commun.*, 2024, **15**, 2995.
29 L. L. Rouhana, M. D. Moussallem and J. B. Schlenoff, *J. Am. Chem. Soc.*, 2011, **133**, 16080–16091.
30 A. Mathew, E. Varghese, S. Choudhury, S. K. Pal and T. Pradeep, *Nanoscale*, 2015, **7**, 14305–14315.
31 F. Vitale, I. Fratoddi, C. Battocchio, E. Piscopiello, L. Tapfer, M. V. Russo, G. Polzonetti and C. Giannini, *Nanoscale Res. Lett.*, 2011, **6**, 1–9.
32 T. Steentjes, P. Jonkheijm and J. Huskens, *Langmuir*, 2017, **33**, 11878–11883.
33 J. Abbou, A. Anne and C. Demaille, *J. Am. Chem. Soc.*, 2004, **126**, 10095–10108.
34 V. Wiwanitkit, *Renal Failure*, 2006, **28**, 101–101.
35 S. Sharma, H. Byrne and R. J. O'Kennedy, *Essays Biochem.*, 2016, **60**, 9–18.
36 G. Ruiz, K. Tripathi, S. Okyem and J. D. Driskell, *Bioconjugate Chem.*, 2019, **30**, 1182–1191.
37 C. M. Michielsen, Y.-T. Lin, J. Yan, A. M. de Jong and M. W. Prins, *ACS Sens.*, 2025, **10**, 2895–2905.
38 L. Heinrich, N. Tissot, D. J. Hartmann and R. Cohen, *J. Immunol. Methods*, 2010, **352**, 13–22.
39 N. C. Marchiando, M. A. Zón and H. Fernández, *Electroanalysis*, 2003, **15**, 40–48.
40 Š. Komorsky-Lovrić and M. Lovrić, *J. Electroanal. Chem.*, 1995, **384**, 115–122.
41 V. Mirceski, S. Komorsky-Lovric and M. Lovric, *Square-wave voltammetry: theory and application*, Springer Science & Business Media, 2007.
42 R. Gesztelyi, J. Zsuga, A. Kemeny-Beke, B. Varga, B. Juhasz and A. Tosaki, *Arch. Hist. Exact Sci.*, 2012, **66**, 427–438.